LA-UR 91 - 165

LA-UR--91-165

DE91 007396

Los Alamos National Laboratory is operated by the University of California for the United States Department of Energy under contract W-7405-ENG-36.

TITLE: Cavity-to-Cavity Interaction in Nucleate Boiling: Effect of Heat Conduction Within the Heater

AUTHOR(S): K. O. Pasamehmetoglu
R. A. Nelson

SUBMITTED TO: 1991 National Heat Transfer Conference
Minneapolis, Minnesota
July 28-31, 1991

DISCLAIMER

MASTER

Los Alamos Los Alamos National Laboratory
Los Alamos, New Mexico 87545

FORM NO 836 R4
ST NO 2629 5/91

DISTRIBUTION OF THIS DOCUMENT IS UNLIMITED

CAVITY-TO-CAVITY INTERACTION IN NUCLEATE BOILING: THE EFFECT OF HEAT CONDUCTION WITHIN THE HEATER

by

Kemal O. Pasamehmetoglu and Ralph A. Nelson

Nuclear Engineering and Technology Division
Los Alamos National Laboratory
Los Alamos, New Mexico 87545

ABSTRACT

This paper presents a numerical study aimed at analyzing bubble behavior as a function of site location. The effects of site distribution on the nucleate boiling curve are examined. Simple local-instantaneous models that mimic the bubble behavior on the boiling surface were implemented into a three-dimensional finite control volume conduction code. For a given site density, sample cases were run for uniform and nonuniform site distribution.

Our results indicate considerable deviation from linearized theories that always assume a uniform distribution. It is shown that bubble emission frequency is a strong function of site location. Consequently, the bubble flux density is shown to deviate from a simple periodic behavior with increasing nonuniformity in site distribution. This study further indicates that a uniform site distribution results in minimum area- and time-averaged surface superheat and minimum temperature variations on the boiling surface. As the distribution becomes less uniform, average surface temperature and surface temperature variations along the boiling surface increase.

NOMENCLATURE

A	Superheat parameter given by Eq. (7) (m-°C)
C_B	Bubble departure diameter correlation constant (dimensionless)
C_M	Microlayer thickness correlation constant (dimensionless)
C_{NC}	Natural convection correlation constant (dimensionless)
C_p	Specific heat (J/kg-K)
D_b	Bubble departure diameter (m)
h	Convective heat-transfer coefficient (W/m^2-K)
h_{fg}	Latent heat (J/kg)
k	Thermal conductivity (W/m-K)
Nu	Nusselt number (dimensionless)
$P(\ )$	Probability density function
Pr	Prandtl number (dimensionless)
R	Bubble radius (m)
R_1	Bubble radius as a result of isobaric growth (m)
R_2	Bubble radius as a result of isothermal growth (m)
Ra	Rayleigh number (dimensionless)
R_b	Bubble departure radius (m)
R_c	Cavity radius (m)
s	Separation distance between adjacent sites (m)
T	Temperature (°C)
T_{sat}	Saturation temperature (°C)
t	Time (s)
t_{end}	Problem end time (s)
z	Axial coordinate (m)
z_b	Elevation of the isotherm passing through nucleus cap (m)
α	Thermal diffusivity (m^2/s)
Δt	Time-step size (s)
ΔT_b	Superheat at bubble cap (°C)
ΔT_c	Superheat at contact (°C)
ΔT_w	Wall superheat (°C)
$\Delta T_{w,o}$	Wall superheat at time bubble starts to grow (°C)
Δx	Octagonal cell diameter (m)
Δz	Axial grid spacing within the heater (m)
Δz_l	Axial grid spacing within the liquid layer (m)

$\Delta\rho$	Density difference between liquid and vapor phases (kg/m^3)
δ	Extrapolated thermal layer thickness (m)
$\Gamma()$	Gamma function
λ	Gamma distribution scaling factor (s^{-1})
ν	Gamma distribution shape parameter (dimensionless)
ρ	Density (kg/m^3)
σ	Surface tension (N/m)
τ	Elapsed time between bubble growth at adjacent sites (s)
τ_d	Bubble growth time (s)

Subscripts

g	Vapor
H	Heater
l	Liquid
max	Maximum
min	Minimum
NC	Natural convection

INTRODUCTION

Nucleate boiling is a highly desirable and thermally efficient mode of thermal energy transport that yields high heat fluxes at reasonable surface temperatures. Therefore, nucleate boiling phenomena have a wide range of applications. Nuclear reactors, chemical plants, and electronic equipment cooling are examples of such applications.

In the last 60 yr, nucleate boiling has been the subject of numerous studies that have yielded both empirical correlations and theoretical models. Unfortunately, the state of the art suggests that almost every experiment calls for a different correlation. To date, even for the simplest boiling configuration (saturated boiling on a horizontal heated plate), we do not have a single correlation that includes all the independent variables of the boiling process. Even the most elaborate correlations cannot be extrapolated outside their data base, and, quite often, within their own data base, an error up to 100% is not surprising when comparing surface heat fluxes for a given wall superheat. For example, Gaertner's (1965) data indicate that $q \sim (\Delta T_w)^{5.5}$. At ~10°C, a scatter of 1°C corresponds to 70% error in surface heat flux. Data scatter within ± 2°C is typically within the repeatability range of most experiments.

We believe a dynamic analysis of bubble nucleation, growth, and departure phenomena is the key to understanding the nucleate boiling process. Many previous investigations have contributed enormously in this area. However, most of these earlier investigations concentrated on predicting the behavior of a single isolated bubble and, having measured the total number of active sites on the surface, extrapolating the results to multiple bubbles. In addition, the single-bubble behavior typically is decoupled from the heater by assuming isothermal surfaces and occasionally constant heat flux surfaces.

There are very few studies in the literature where bubble-to-bubble or cavity-to-cavity interactions are considered. These studies are aimed mostly at studying the interaction of a pair of adjacent sites. The effect of multiple neighboring cavities on bubble behavior and, ultimately, on the boiling curve is not fully understood yet. The present study is aimed at further understanding of one piece of the puzzle, that is, the thermal interaction between cavities through heat conduction within the solid. Theoretically, the nucleation sites may interact through a number of mechanisms: (a) sonic waves generated

during the early bubble growth and departure stages, which is postulated to promote nucleation; (b) hydrodynamic interaction because of liquid motion, pressure changes, and convective heating during the bubble growth and departure, which may promote or inhibit nucleation; (c) seeding, which is only valid for cavities in the very near vicinity of a growing bubble and which may promote intermittent activations; and (d) thermal interaction through heat diffusion within the heated solid, which may promote or inhibit nucleation. The available literature is reviewed briefly in the next section.

LITERATURE REVIEW

Based on an analysis of high-speed motion pictures, Henley and Hummel (1967) concluded that nucleation of a bubble at one site inhibited nucleation at all surrounding sites for a brief period thereafter. They also observed a strong tendency for bubble formation at the surrounding sites following the departure of the central bubble. Sonic interaction between the growing bubbles was postulated to be responsible for this behavior.

Chekanov (1977) experimentally studied the interaction of two adjacent cavities using boiling water at atmospheric pressure. Chekanov monitored the time elapsed between the start of bubble growth from two adjacent artificial cavities on a 20-mm-thick permalloy plate. The plate was heated by two copper electrodes that could be moved relative to each other so that the distance between the cavities could be varied. Chekanov found that the time elapsed between the growth of the two bubbles followed a gamma distribution in the form

$$P(\tau) = \frac{\lambda(\lambda\tau)^{\nu-1} e^{-\lambda\tau}}{\Gamma(\nu)} \quad , \tag{1}$$

where λ and ν are the scaling and shape parameters, respectively. For a distance between cavities less than 3 departure diameters, Chekanov observed that ν is greater than 1. This was interpreted as a sign for "repulsive" interaction, when the growth of a bubble at one site inhibited the growth of the bubble at the adjacent site. At distances greater than 3 bubble diameters, the interaction was postulated to be "attractive," such that the growth of one bub-

ble enhanced the growth at the adjacent site. At distances much larger than bubble diameter ($s / D_b \sim 10$), there were no interactions ($\nu = 1$). Chekanov postulated that the results could be explained by sonic interactions. This appears to contradict their claim that, at short distances, there is a repulsive interaction, whereas sonic interactions are expected to enhance the bubble growth.

Calka and Judd (1985) boiled dichloromethane on a coated glass surface and observed bubble growth from adjacent sites. They found that the time elapsed between the growth of two adjacent bubbles followed a Gamma distribution, where the shape parameter vs the separating distance curve was in qualitative agreement with Chekanov's plot. However, quantitatively, Calka and Judd observed that ν was greater than 1 for separating distances less than 1 bubble diameter. Between 1 and 4 bubble diameters, ν was observed to be less than 1. Beyond 4 diameters, ν was equal to 1. However, the disagreement between the two studies is mostly in the interpretation of the results. Calka and Judd postulated that $\nu > 1$ corresponds to a "attractive" interactions, whereas $\nu < 1$ represents a "repulsive" interaction. The mechanism for attractive interaction was postulated to be the seeding mechanism, where the growing bubble in one cavity activates a surrounding cavity intermittently through vapor seeding, based on the observations of Judd and Lavdas (1980).

More recently, Judd (1988) provided some more data using dichloromethane boiling over a glass surface. In this experiment, the heating surface was different than the one used by Calka and Judd (1985). Apparently, the older surface had twice as many active cavities as the new one. A Gamma distribution fit to the new data showed that ν was greater than 1 for separating distances less than a bubble diameter. Beyond this distance, there were no interactions between the sites as ν remained constant and equal to 1.

As indicated by Sultan and Judd (1983), the bubble flux density distribution over a heating surface is also an indirect indication for nucleation phenomenon and possible interactions. Their study (Sultan and Judd, 1978) indicated that sites are distributed in cluster forms over the heating surface, which suggests that bubble formation may promote activation in the neighboring sites, contrary to Chekanov's postulate. To examine this phenomenon further, Sultan and Judd (1983) obtained data using boiling water at atmospheric pressure, heated by a copper block 6 in. (15.24 cm) in diameter, reduced to 2 in. (5.08 cm) at the boiling surface. Using a bubble detection probe, they obtained

the time elapsed between the bubble formation at two adjacent sites. The reduced data are shown in Fig. 1. As shown in this figure, the elapsed time remains constant for saturated boiling at distances greater than ~5 mm. For distances shorter than this critical separation distance, the elapsed time decreases with decreasing distance. This critical separation distance appears to decrease with increasing subcooling.

Sultan and Judd (1983) recommended that this behavior could be explained through radial heat conduction within the heater. They postulated that the superheated liquid near the bubble base will act as an instantaneous ring source following the bubble departure. This requires that the heater temperature at this instance be lower than the liquid temperature, and all the liquid superheat is diffused instantaneously into the heating surface. Calculating the speed of propagation of the instantaneously supplied sensible heat in the radial direction, they estimated the following relation:

$$s - R_b \cong 0.57\sqrt{\tau - \tau_d} \quad , \tag{2}$$

which yielded a reasonable agreement with the data. However, they were not able to measure the bubble departure radius, R_d, and the growth period τ_d, required in Eq. (2). These quantities had to be estimated from literature-based models (Sultan, 1981), the accuracy of which is questionable when applied to their experimental conditions. Furthermore, the instantaneous ring source model is in contradiction with some commonly accepted criteria in boiling heat transfer, such that (i) the liquid superheat can not exceed the wall superheat and (ii) following bubble departure, cold liquid from the bulk comes into contact with superheated wall and the subsequent heating of the liquid determines the bubble waiting time (Hsu, 1962). It is conceivable that the time-dependent heat-transfer coefficient under a waiting and growing bubble acts as a transient source and sink term, which alters the thermal behavior in the vicinity. This is the essence of thermal site interaction. However, compared with this scenario, the model proposed by Sultan and Judd seems highly exaggerated. Furthermore, the model of Sultan and Judd is independent of the adjacent bubble history, as well as of the existence of other cavities. The square root relationship suggested by Eq. (2) is more likely to suggest a hydrodynamic interaction than a thermal one.

In summary, these experimental data possibly include the effects of all of the interaction mechanisms cited in the introduction. However, all the mechanisms are not necessarily important within the same data set. For example, the thermal interaction is not expected to be the dominant one in the studies of Chekanov (1977), Calka and Judd (1985), and Judd (1988). These experimental data were obtained using a very thin boiling surface (in case of Chekanov) or glass surfaces (Calka and Judd, 1985; Judd, 1988), where the horizontal heat conduction is very restricted. In these studies, sonic and hydrodynamic mechanisms are likely to dominate. On the other hand, thermal interactions may become important in the study of Sultan and Judd (1983), where a copper block is used as the heating surface. In fact, Sultan and Judd claim thermal interactions are the only important mechanism. We question this claim and suggest that other mechanisms may be equally responsible for these data.

The present study is aimed at investigating the thermal interactions within the heater only. Our current closure relationships do not permit us to look into other types of interactions, such as sonic and hydrodynamic interactions. Therefore, the present study is not aimed at analyzing any data set cited above. The study is expected to isolate the thermal interaction problem and examine the consequences of such interaction on the boiling curve. Once again, we believe that a comprehensive model accounting for other types of interactions is necessary to explain the existing data.

In the next section, we will describe our computer model specifically developed to analyze the heater conduction effects on cavity-to-cavity interaction in nucleate boiling.

MODEL DESCRIPTION

Heater Analysis of Nucleation Dynamics (HANDY) is a three-dimensional, implicit-explicit, finite-volume, conduction-heat-transfer computer program that we are developing to analyze the nucleate boiling process. The finite control volumes are octagonal and square cylinders. Figure 2 illustrates the mesh structure. Each octagonal cell on the heater surface ($z = 0$) may contain a nucleation site (not necessarily active). The cell size in the horizontal direction is typically on the order of a bubble departure diameter (~ 1 mm), whereas the cell height can be made very small, depending on the heater

thickness. The time-step size is on the order of a fraction of a millisecond because the phenomena of interest such as bubble waiting time and growth time are typically several milliseconds. Under these restrictions, the axial cell size limits the program stability. Thus, the code is made implicit-explicit in the axial direction with a degree of implicitness 0.5, which provides an unconditional stability in the axial direction. The solution scheme is fully explicit in the horizontal direction because the cell and the time-step sizes of interest do not violate the stability criterion. Furthermore, this scheme provides an easier coupling between octagonal- and square-cell temperature fields and results in a tridiagonal matrix that yields a computationally more efficient solution than a fully implicit case. Further details on the HANDY code can be found in Pasamehmetoglu and Nelson (in preparation).

The boiling surface is characterized by a local (cell-averaged) and instantaneous (averaged over the time-step size) heat-transfer coefficient that satisfies the required boundary condition for the conduction solution. The coupling is time-wise explicit for the surface temperature dependence of the heat transfer coefficient. Version 1 of HANDY is only applicable to saturated water boiling at atmospheric pressure. The bubble behavior is simulated using literature-based models, which were reformulated (when necessary) to yield local-instantaneous heat transfer coefficients. Symmetry conditions supply other needed boundary conditions.

The current computer model is applicable to the discrete bubble region of nucleate boiling curve. There are numerous cavities on the boiling surface, some of which are activated and generate bubbles. Underneath the growing bubble and within its vicinity, latent heat transport and enhanced convection are important. In the region of these bubbles, the surface is cooled by natural convection to single-phase liquid. Likewise, the heat-transfer mechanisms change locally as a function of time because of various stages in bubble dynamics. For example, the mechanism during the bubble waiting time is different than the mechanism during growth. Thus, the computer model requires various closure relationships that will provide the heat-transfer coefficients as a function of location and time. In the following subsections, these closure relationships are summarized.

Natural Convection Model. The surface cells without active cavities are assumed to be cooled by natural convection. For these cells, the well-known heat-transfer correlation given by

$$Nu = C_{NC}\ Ra^{1/3} \tag{3}$$

is used (Holman, 1981) to predict the extrapolated thermal layer thickness under natural convection conditions. The advantage of this correlation is that when it is written in terms of the heat-transfer coefficient, h_{NC}, it is independent of characteristic length. The proportionality constant C_{NC} currently is set to 0.15. This is a commonly accepted magnitude for isothermal surfaces, even though values as high as 0.6 have been reported in the literature. Thus, knowing the value of the heat-transfer coefficient, the extrapolated thermal layer thickness can be estimated as

$$\delta_{T,NC} = \frac{k_l}{h_{NC}} \tag{4}$$

Then, the local instantaneous heat-transfer coefficient is obtained through one-dimensional transient conduction solution within the liquid layer. The governing equation becomes

$$\frac{\partial T_l}{\partial t} = \alpha_l \frac{\partial^2 T_l}{\partial z^2} \tag{5}$$

with the following initial and boundary conditions:

$$@\ t = 0, \qquad T_l = T_{sat}$$

$$@\ z = 0, \qquad T_l = T_w(x, y, t)$$

$$@\ z = \delta_{T,NC}, \qquad T_l = T_{sat}$$

In the code, the solution to this transient problem is obtained numerically using the thermal thickness in user-defined axial cells. The solution scheme is fully implicit; however, the transient boundary temperature, $T_w(x,y,t)$, is the old time-temperature from the heater solution.

Cavity Activation Criterion. The user can define the desired number of cavities (limited to one cavity per surface cell) and cavity radii in the octagonal surface cells. The criterion used for the activation of this cavities is determined based on the theory developed by Han and Griffith (1965). Based on a maximum extrapolated thermal layer thickness, δ_{NC}, the range of cavities that can be activated in saturated liquids may be obtained from

$$R_{\substack{c,\max \\ c,\min}} = \frac{\delta_{T,NC}}{3}\left(1 \pm \sqrt{1 - \frac{6A}{\delta_{T,NC}\ \Delta T_{w,NC}}}\right) \quad , \tag{6}$$

where

$$A = \frac{2\sigma T_{sat}}{\rho_g h_{fg}} \quad . \tag{7}$$

The cavities with radii between $R_{c,max}$ and $R_{c,min}$ will be activated. However, study of Shoukri (1974) show that, on natural surfaces, cavities with sizes closer to the lower range are present and will be activated.

Bubble Departure Criterion. Currently, a simple bubble departure criterion is used such that a fixed departure diameter determines the departure condition. We used the correlation of Cole and Rohsenow (1969), which is given by

$$D_b = C_B \sqrt{\frac{\sigma}{g\ \Delta\rho}} \left(\frac{\rho_l C_{p,l} T_{sat}}{\rho_g h_{fg}}\right)^{5/4} \quad , \tag{8}$$

where $C_B = 1.5 \times 10^{-4}$ is recommended for water. For the calculations reported in this paper, we used $C_B = 1.25 \times 10^{-4}$, which yields a bubble departure diameter of 2 mm for saturated water at atmospheric pressure. This number was more suitable for number density estimates needed for the present calculations.

Bubble Waiting Time Models. According to Hsu (1962) and Han and Griffith (1965), the bubble from an active cavity will grow if the liquid tem-

perature at the bubble cap location reaches the required superheat. For a hemispherical nucleus emerging from a cavity, the required superheat can be calculated from

$$\Delta T_b = \frac{A}{R_c} \quad . \tag{9}$$

According to Han and Griffith, the isotherm tangent to the bubble cap will be located at a vertical location,

$$z_b = \frac{3}{2} R_c \quad , \tag{10}$$

relative to the heating surface, a short lateral distance away from the nucleus.

After bubble departure, bulk liquid comes into contact with the heater surface, and the thermal boundary layer starts developing. The development of the thermal boundary layer, δ_T, may be obtained from the solution of the transient conduction equation in the liquid given by Eq. (5). However, if z_b is less than the nodal spacing, Δz_l, for the numerical solution of Eq. (5) (quite often true because the cavity radii are typically on the order of μm), then an approximate approach is used as

$$\delta_T(t) = \sqrt{\pi \alpha_l t} \quad . \tag{11}$$

This is the well-known solution for extrapolated thermal layer thickness in a semi-infinite solid for a constant boundary temperature. The instantaneous temperature at location z_b is calculated through

$$\Delta T_l(z_b, t) = \Delta T_w(t)\left[1 - \frac{z_b}{\delta_T(t)}\right] \quad , \tag{12}$$

where the quasi-steady assumption is invoked by using the instantaneous wall temperature. If the temperature calculated in Eq. (12) exceeds ΔT_b from Eq. (9), the bubble starts growing.

During the waiting time, except during the first time-step size following bubble departure, the convective heat-transfer coefficient is computed from the numerical solution in the liquid field as

$$h = - k_l \frac{\left(\frac{\partial T_l}{\partial z}\right)_{z=0}}{\Delta T_w(t)} \quad . \tag{13}$$

if $z_b > \Delta z_l$. Otherwise, the convective heat-transfer coefficient is calculated as

$$h = \frac{k_l}{\delta_T} \quad . \tag{14}$$

For the first time-step size following bubble departure, a quench heat-transfer coefficient is required. The instantaneous contact temperature for two semi-infinite solids at uniform temperature is given by

$$\Delta T_c = \Delta T_w \left(1 + \sqrt{\frac{k_l C_{p,l} \rho_l}{k_H C_{p,H} \rho_H}} \right)^{-1} \quad . \tag{15}$$

In our problem, the heater has a certain temperature distribution in the axial and lateral directions. Knowing the contact temperature, the finite control volume equations are solved to obtain a value of h_1 that would yield a cell temperature equal to the contact temperature. Similarly, a heat-transfer coefficient, h_2, that would result in a liquid contact temperature to that given by Eq. (15) within one time-step size is calculated. The maximum of the two magnitudes, h_1 and h_2, is chosen as the quench heat-transfer coefficient.

Bubble Growth Time Models. Isobaric and isothermal growth equations are considered for the bubble growth rate. For the isobaric growth, the modified Rayleigh solution provided by VanStralen *et al.* (1975) is used. This growth equation is given by

$$R_1(t) = 0.8165\, t \sqrt{\frac{\rho_g h_{fg} \Delta T_{w,o}\, e^{-\sqrt{t/\tau_w}}}{\rho_l T_{sat}}} \quad , \tag{16}$$

where $\Delta T_{w,o}$ is the wall superheat at the time bubble starts growing and τ_w is set to 10 ms when used within this equation. For the isothermal growth, the bubble is assumed to grow due to microlayer evaporation. Assuming conduction across the microlayer of average thickness $\delta_o/2$, the energy equation yields

$$\frac{d R_2}{d t} = \frac{k_l \Delta T_w(t)}{\rho_g h_{fg} \delta_o(t)} \quad , \tag{17}$$

where the initial microlayer thickness is formulated as (Olander and Watts, 1969)

$$\delta_o = C_M \frac{\rho_g h_{fg}}{\rho_l C_{p,l} \Delta T_w} \sqrt{Pr_l}\; R_2(t) \quad . \tag{18}$$

Note that this formulation yields $R_2 \sim t^{1/2}$, which typically characterizes the asymptotic bubble growth. For these calculations, we set $C_M = 1.6$. For the isothermal growth, we neglected the effect of relaxation microlayer suggested by VanStralen *et al.* (1975). Lee and Nydahl's study (1989) indicates that the liquid isotherms do not surround the bubble during asymptotic growth. The isotherms fold within a thin layer near the bubble base. Thus, the contribution of relaxation microlayer would be minimal. The isothermal and isobaric growth equations are combined using the approach suggested by VanStralen *et al.* (1975) as

$$R(t + \Delta t) = R(t) + \frac{d}{d t}\left[\frac{R_1(t)\, R_2(t)}{R_1(t) + R_2(t)}\right] \Delta t \quad . \tag{19}$$

The bubble is assumed to depart when the radius exceeds the departure radius discussed earlier.

The heat-transfer coefficient during bubble growth is calculated through quasi-steady conduction across the microlayer. Underneath the growing bubble, the average microlayer thickness is assumed to be $\delta_o/2$, whereas the average extrapolated thermal layer thickness is set to δ_o outside the growing bubble. Thus the cell-averaged heat-transfer coefficient is given by

$$h(t) = \frac{k_l}{\delta_o R_d^2}\left[2R^2 + \left(R_d^2 - R^2\right)\right] \quad . \tag{20}$$

Further details and discussion of these models can be found in the report by Pasamehmetoglu and Nelson (1991). Using the HANDY code, which contains the above-described models, we looked at a sample problem for nucleation dynamics. The sample problem is described in the following section.

SAMPLE PROBLEM DESCRIPTION

As a sample problem, we looked at the boiling of saturated water at atmospheric pressure. A 1-mm-thick copper plate was chosen as the heater material. The heater was supplied with a constant heat flux boundary condition of 70 kW/m^2 at the lower surface. If we look at Gaertner's (1965) and Sultan's (1977, 1981) boiling curves, the expected average surface temperature is between 10 and 12°C for these conditions. We assumed a number density, N/A = 61,695 active sites per m^2, which was held constant for all cases studied. Note that Gaertner's (1965) number density data yield about 46,000 sites/m^2, Sultan's (1977) data yield 85,000 sites/m^2,and Shoukri's (1974) data yield 155,000 sites/m^2. Thus, the number used in this study is between Sultan's and Geartner's measurements. The present study concentrates on the effects of site location. To isolate the problem, the additional effects of cavity-size variations were eliminated and will be considered in the future. All the cavities were assumed to be identical and to have cavity radii of 3.5 μm.

The imposed heat flux would yield a surface superheat of 38.4°C under natural convection conditions, which corresponds to an extrapolated thermal layer of 373.4 μm. For this value of the thermal layer thickness and the wall

superheat, the cavity radii range that can be activated was calculated to be between 0.85 and 248.1 μm. Thus, the chosen cavity radius of 3.5 μm is closer to the minimum magnitude of cavity radii that can be activated.

The diameter of the octagonal cells was set equal to the bubble departure diameter. The numerical parameters used for the current calculations are given in Table 1. Using the same numerical parameters, we ran five sample cases by changing the nucleation site locations. Figure 3 illustrates all five cases. Note that for a constant number density, Case 1 corresponds to a uniform site distribution, whereas Case 5 is the most nonuniform one among the five cases considered. The results of the calculations for these cases are given in the following section.

RESULTS

Case 1 corresponds to a uniform cavity distribution over the heating surface for a given number density. In this case, the bubble reaches a steady-period of 19.5 ms, as shown in Fig. 4. All the bubbles on the surface would be in phase, which is illustrated by the bubble flux ratio shown in Fig. 5. The bubble flux ratio is defined as the number of bubbles growing on the surface divided by the number of active cavities. As shown in Fig. 5, for a uniform distribution, bubble flux ratio is periodic and is either one or zero.

Case 2 corresponds to a small deviation from a uniform distribution as a pair of adjacent cavities have a separating distance equal to 1 bubble diameter. In this case, site number 1 generates bubbles with a frequency of 46.5 Hz, whereas site number 2 generates bubbles with a frequency of 55.6 Hz, as shown in Fig. 6. The behavior of individual bubbles is expected to be periodic.

TABLE 1
NUMERICAL PARAMETERS USED IN THE CURRENT CALCULATIONS

Δz (m)	Δx (m)	Δz_l (m)	Δt (s)	t_{end} (s)
1.0×10^{-4}	2.013×10^{-3}	3.734×10^{-5}	5.0×10^{-4}	2.5

The numerical calculations indicate a small deviation from periodic behavior, as the waiting time for bubble 2 occasionally decreases from 8.5 ms to 8 ms. This is possibly a consequence of the numerical integration using 0.5-ms time-step sizes and is not caused by a system nonlinearity. However, the boiling surface behavior has a higher order periodicity. One way of characterizing the surface behavior would be again to look at bubble flux ratio. Figure 7 illustrates the bubble flux ratio for this case over a 200-ms time-frame. As shown, the behavior is not periodic in this time frame. However, the patterns will repeat themselves every 387 ms. Thus, the period for the bubble flux ratio increases by nearly 20 times as compared with Case 1.

Case 3 represents a combination of Cases 1 and 2. In this case, all four bubbles are out of phase, as shown in Fig. 8. However, bubbles generated from sites 2 and 3 are out of phase but have the same period of 19.5 ms. Bubbles emitted from site 1 have the longest period (22 ms), whereas site 4 generates bubbles with period of 17.5 ms. Figure 9 illustrates the bubble flux ratio for this case over a time frame of 100 ms. The bubble flux ratio patterns are expected to repeat themselves with a period of 7.5 s, which is 385 times the period of uniform distribution (Case 1).

Cases 4 and 5 increase the cavity distribution nonuniformity even further. For Case 4, sites 1 and 4 are symmetric and generate bubbles with a frequency of 50 Hz. Bubbles emitted by site 3 have the highest frequency (60.6 Hz), whereas bubbles generated by site 2 have the lowest frequency (40 Hz). Finally, Case 5 has the highest degree of nonuniformity among all five cases that we considered. Sites 2 and 3 are symmetric and have a bubble emission frequency of 50 Hz. Sites 1 and 4 emit bubbles with frequencies of 40.8 Hz and 58.8 Hz, respectively. The bubble flux ratios for Cases 4 and 5 have a pattern repeat period of 8.25 s and 8.33 s, respectively. Figures similar to those for Cases 1 through 3 can be generated for these cases as well. For brevity, they are not included in the paper. Thus, it can be concluded that the heater surface characteristics, characterized by the bubble flux ratio in this study, become more and more nonlinear as the nonuniformity in cavity distribution increases. It would be interesting to see the effects of this behavior on the boiling curve.

Figures 10 through 14 illustrate the area-averaged instantaneous surface superheat, instantaneous maximum surface superheat, and instantaneous minimum surface superheat for Cases 1 through 5,

respectively. As shown, the surface-averaged wall superheat and the maximum wall superheat increase as the site distribution becomes less uniform (as we go from Case 1 to Case 5). On the other hand, increasing the nonuniformity decreases the minimum surface superheat, thus, creating a larger temperature scatter on the boiling surface. Time- and area-averaged temperatures typically are used for plotting the boiling curve. We obtained the time-averaged values by averaging the data over the last second of the 2.5-s run, and these are reported in Table 2. Note that for Cases 3 through 4, bubble flux repeat periods are much larger than a second; thus, time-averaging done over a second does not really represent an appropriate average. However, the obtained values is expected to be within ±0.05°C of the exact value.

SUMMARY AND CONCLUSIONS

In this paper, we studied the effect of the distribution of active sites on the bubble behavior and its consequences on the boiling curve. A three-dimensional conduction computer program is being developed for analyzing the nonlinear effects of site-to-site interactions. The HANDY computer program has various models that mimic bubble behavior on a boiling surface. The current version contains literature-based simple models for these purposes. These models were described briefly in this paper.

TABLE 2
TIME-AVERAGED WALL SUPERHEATS

Case	Time and Area Averaged Wall Superheat	Time Averaged Maximum Superheat	Time Averaged Minimum Superheat
1	10.30	10.52	9.82
2	10.54	11.11	9.66
3	10.68	11.36	9.50
4	10.78	11.84	9.50
5	10.85	11.98	9.50

The code is applied to a simple boiling configuration in which the surface contains a number of identical cavities. The distribution of these cavities is changed while keeping the number density the same. The distributions from totally uniform to highly nonuniform cases were considered in five separate cases. Using symmetry boundary conditions, the total number of active cavities was kept at maximum four. However, more cavities can be analyzed easily using the existing code. All cases are run using a copper heater, which is commonly treated in the literature as an isothermal surface.

Even with the small perturbations tried in these five cases, the results indicated considerable deviation from linearized theories. For example, it was shown that bubble waiting time is not only a function of average surface temperature and cavity size but also a strong function of the cavity location. Within the parametric range of this study and while keeping the cavity size and heating conditions the same, we were able to show that there is up to a 55% change in waiting time. Similarly, the periodic behavior of the bubble flux density becomes highly complex if the site distribution deviates from uniform. It also was shown that the site distribution has a noticeable influence on the time- and area-averaged wall temperatures. This is the quantity typically used in plotting the boiling curve. The average temperature shows an increase as the site distribution becomes increasingly nonuniform. Within the parametric range of this study, which is restricted to a maximum of four sites, the maximum deviation was a little larger than 0.5°C. For a boiling curve of saturated water at atmospheric pressure, this is considerable as it typically translates to more than 30% scatter in the corresponding heat flux estimates. Likewise, a nonuniform distribution promotes a larger span between the minimum and maximum surface temperatures.

Note that the present model represents a small perturbation from linearized models. Nevertheless, it presents strong indications that the actual nucleate boiling phenomenon is highly nonlinear. We must note that the results presented within the paper do not account for cavity-size variations, which are present in real systems. These effects are observed to enhance the nonlinear behavior and will be included in the future studies. As the next step in our modeling efforts, we will incorporate a more dynamic bubble growth model into HANDY. This model will include an instantaneous force balance on the bubble and does not require an *a priori* knowledge of the bubble departure diameter. Also, the effects of hydrodynamic interactions are

being incorporated into the code by considering the fluid convective velocities and pressure variations resulting from bubbles' motion. Techniques to identify and analyze nonlinear and chaotic behavior also will be integrated into the interpretation of the results in an effort to better understand the behavior.

REFERENCES

Calka, A., and Judd, R. L., 1985, "Some Aspects of the Interaction among Nucleation Sites During Saturated Nucleate Boiling," *Int. J. Heat Mass Transfer* **28**, 2331-2342.

Chekanov, V. V., 1977, "Interaction of Centers in Nucleate Boiling," translated from *Teplofizika Vysokikh Temperatur* **15**(1), 121-128.

Cole, R., and Rohsenow, W. M., 1969, "Correlation of Bubble Departure Diameters for Boiling of Saturated Liquids," *Chem. Eng. Prog. Symp. Series* **92**(65), 211-213.

Gaertner, R. F., 1965, "Photographic Study of Nucleate Boiling on a Horizontal Surface," *Trans. ASME, J. Heat Transfer* **87**, 17-29.

Han, C-Y and Griffith, P., 1965, "Mechanisms of Heat Transfer in Nucleate Pool Boiling, Part 1: Bubble Initiation, Growth and Departure," *Int. J. Heat Mass Transfer* **8**, 887-904.

Henley, J. J. and Hummel, R. L., 1967, "A Third Factor in Boiling Nucleation," *Industrial and Engineering Chemistry, Fundamentals* **6**,(4), 603-606.

Holman, J. P., 1981, *Heat Transfer*, 5th edition (McGraw-Hill, New York).

Hsu, Y. Y., 1962, "On the Size Range of Active Nucleation Cavities on a Heating Surface," *Trans. ASME, J. Heat Transfer* **84**, 207-216.

Judd, R. L., 1988, "On Nucleation Site Interaction," *Trans. ASME, J. Heat Transfer* **110**, 475-478.

Judd, R. L., and Lavdas, 1980, C. H., "The Nature of Nucleation Site Interaction," *Trans. ASME, J. Heat Transfer* **102**, 461-464.

Lee, R. C. and Nydahl, J. E., 1989, "Numerical Calculation of Bubble-Growth in Nucleate Boiling From Inception Through Departure," Trans. ASME, J. Heat Transfer **111**, 474-479.

Olander, R. R. and Watts, R. G., 1969, "An Analytical Expression of Macrolayer Thickness in Nucleate Boiling," *Trans. A ME, J. Heat Transfer*, Vol. 91, pp. 178-180.

Pasamehmetoglu, K. O. and Nelson, R. A., 1991, "A Finite Control Volume Computer Program for Heater Analysis of Nucleation Dynamics - HANDY, Version 1.0," Los Alamos National Laboratory report in preparation.

Shoukri, M., 1974, "Nucleation Site Activation in Saturated Boiling," Master Thesis, McMaster University, Hamilton, Canada.

Sultan, M., 1977, "Spatial Distribution of Active Sites and Bubble Flux Density," Master Thesis, McMaster University, Hamilton, Canada.

Sultan, M., 1981, "Interaction of the Nucleation Phenomena at Adjacent Sites in Nucleate Boiling," Ph.D. Thesis, McMaster University, Hamilton, Canada.

Sultan, M. and Judd, R. L., 1978, "Spatial Distribution of Active Sites and Bubble Flux Density," *Trans. ASME, J. Heat Transfer* **100**, 56-62.

Sultan, M. and Judd, R. L., 1983, "Interaction of Nucleation Phenomena at Adjacent Sites in Nucleate Boiling," *Trans. ASME, J. Heat Transfer* **105**, 3-9.

VanStralen, S. J. D., Sohal, M. S., Cole, R., and Sluyter, W. M., 1975, "Bubble Growth Rates in Pure and Binary Systems: Combined Effect of Relaxation and Evaporation Microlayer," *Int. J. Heat Mass Transfer* **18**, 453-467.

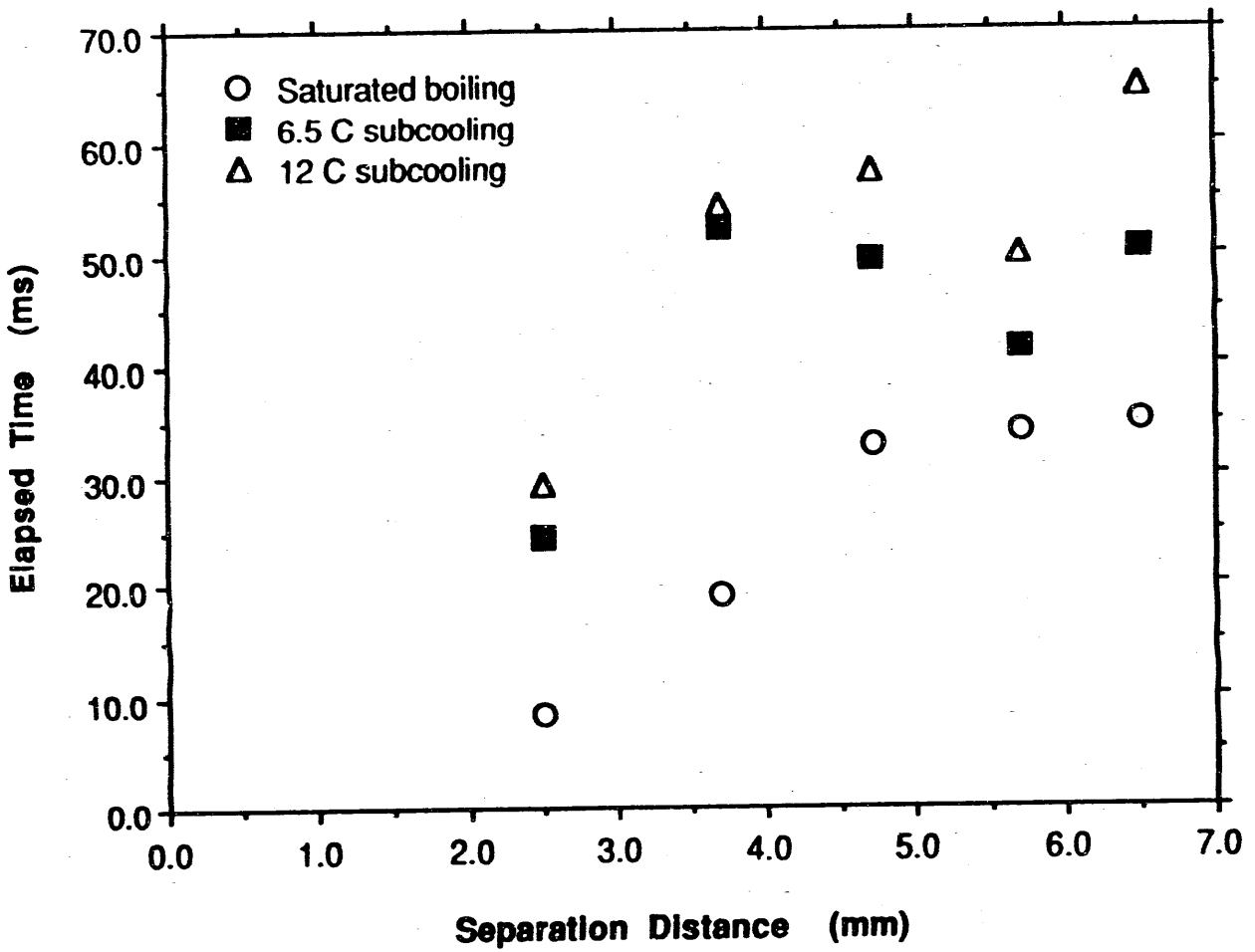

Fig. 1. Elapsed time vs separating distance date of Sultan (1981).

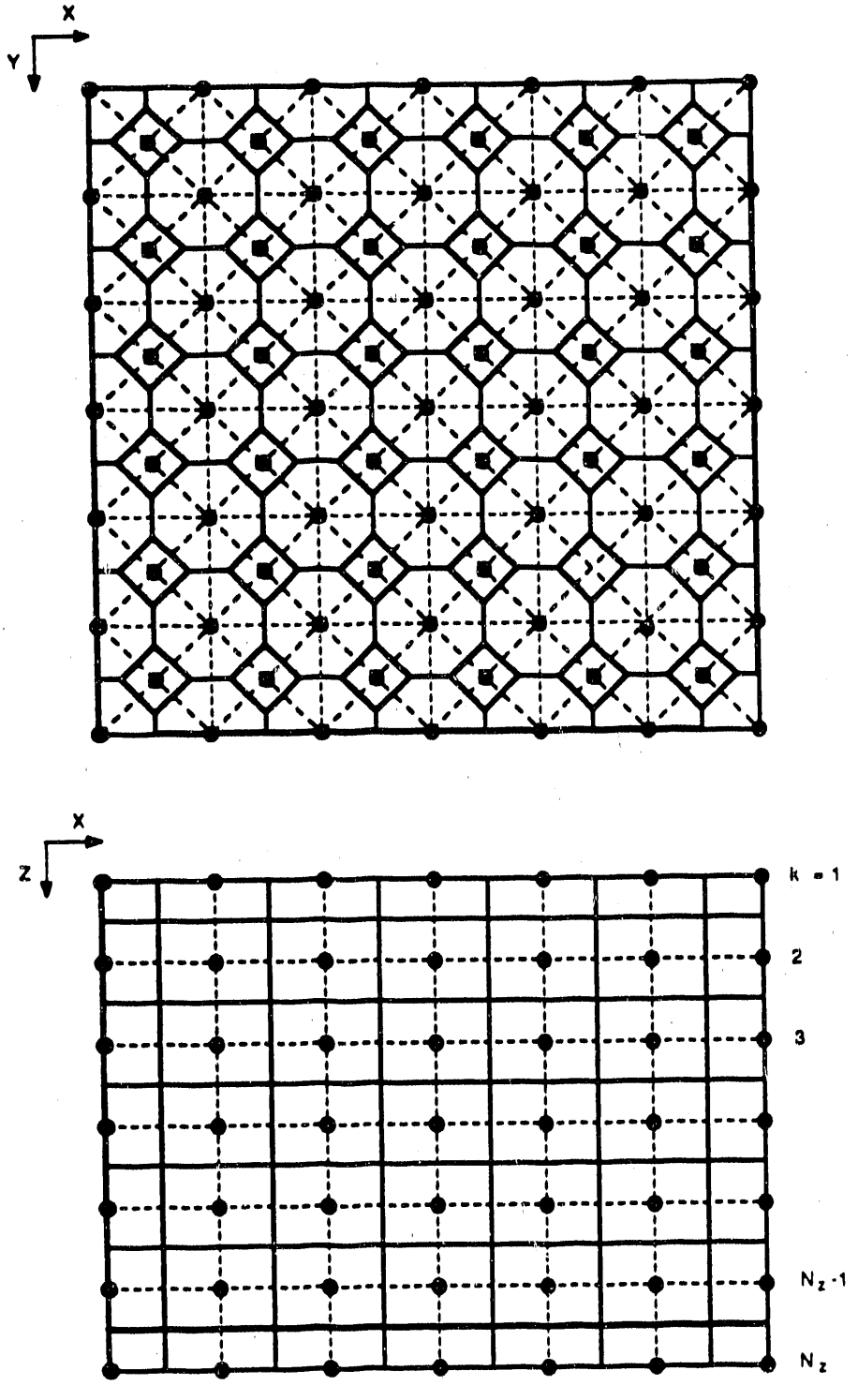

Fig. 2. Mesh structure of HANDY.

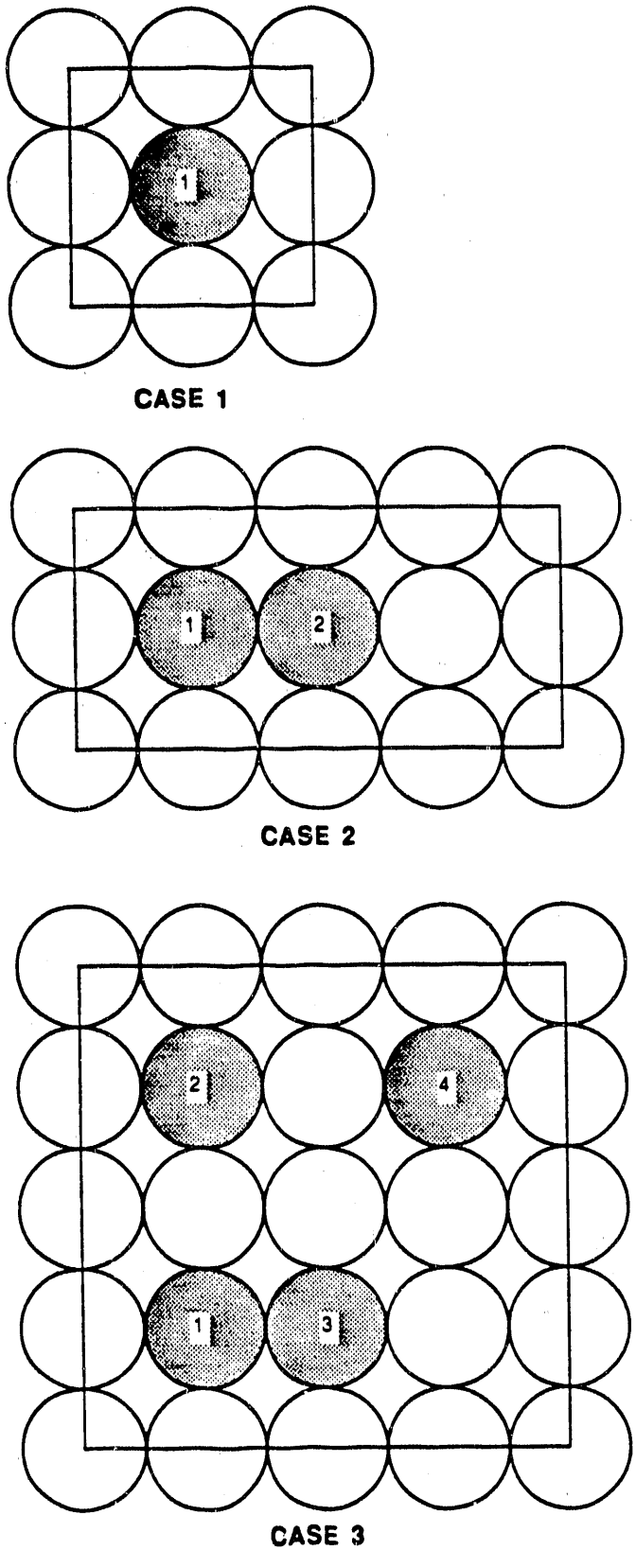

Fig. 3. Various site distribution cases examined in this study.

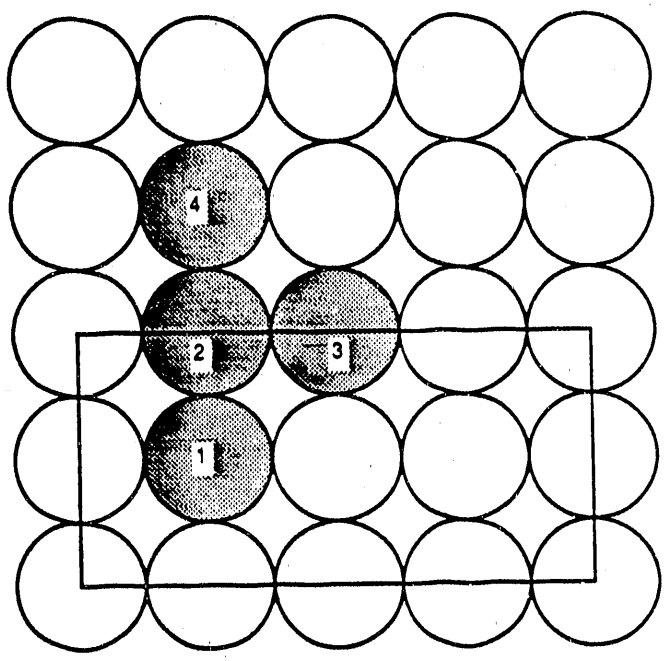

CASE 4

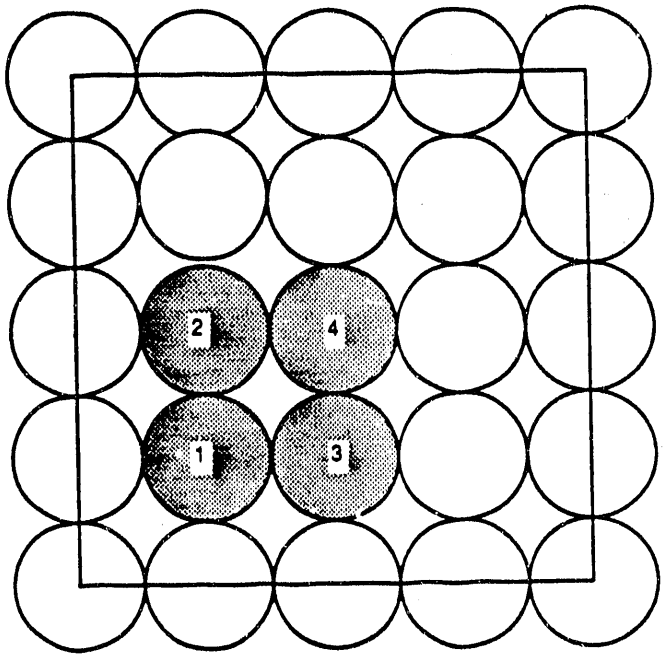

CASE 5

Fig. 3. (cont)

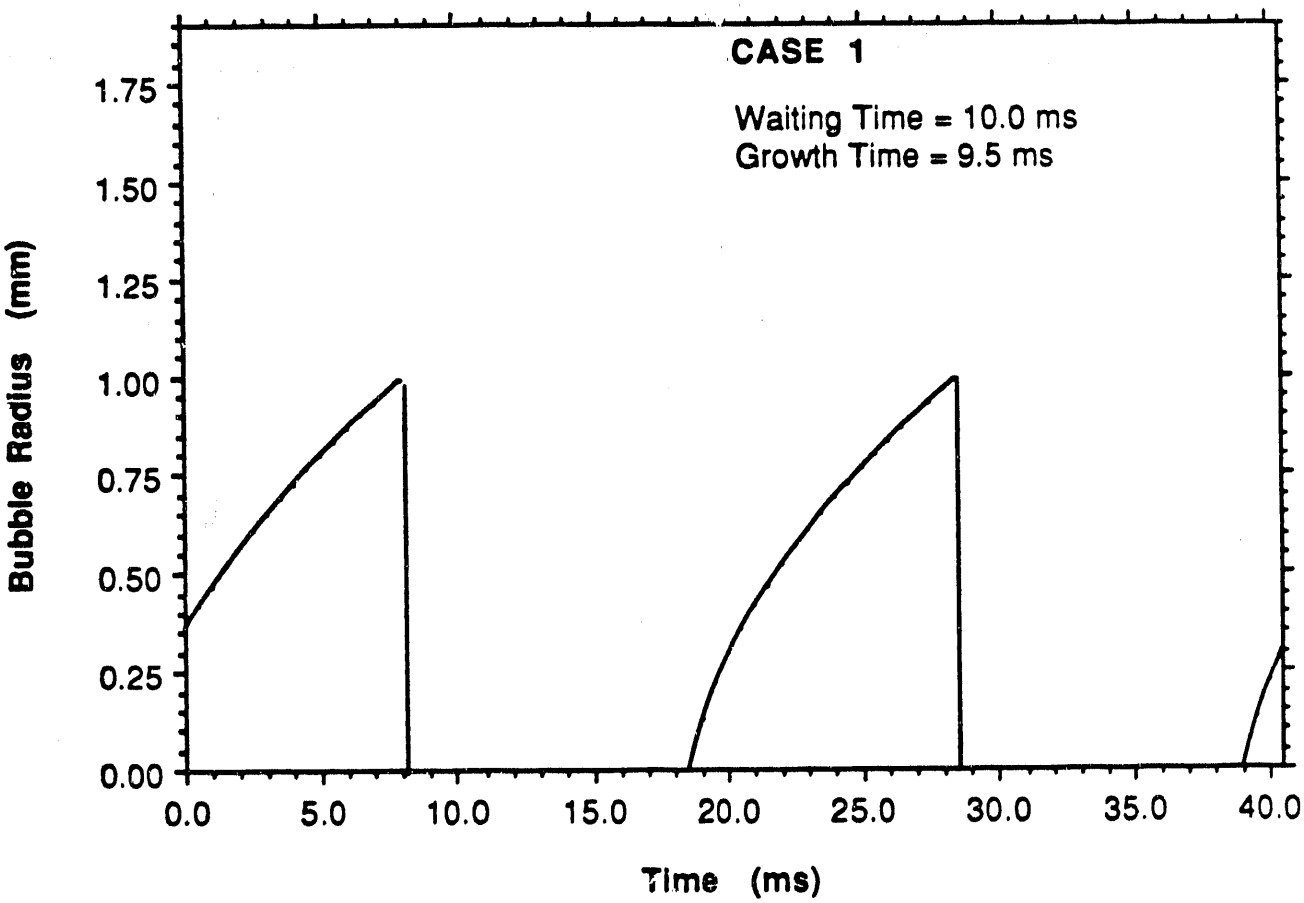

Fig. 4. Bubble behavior for Case 1.

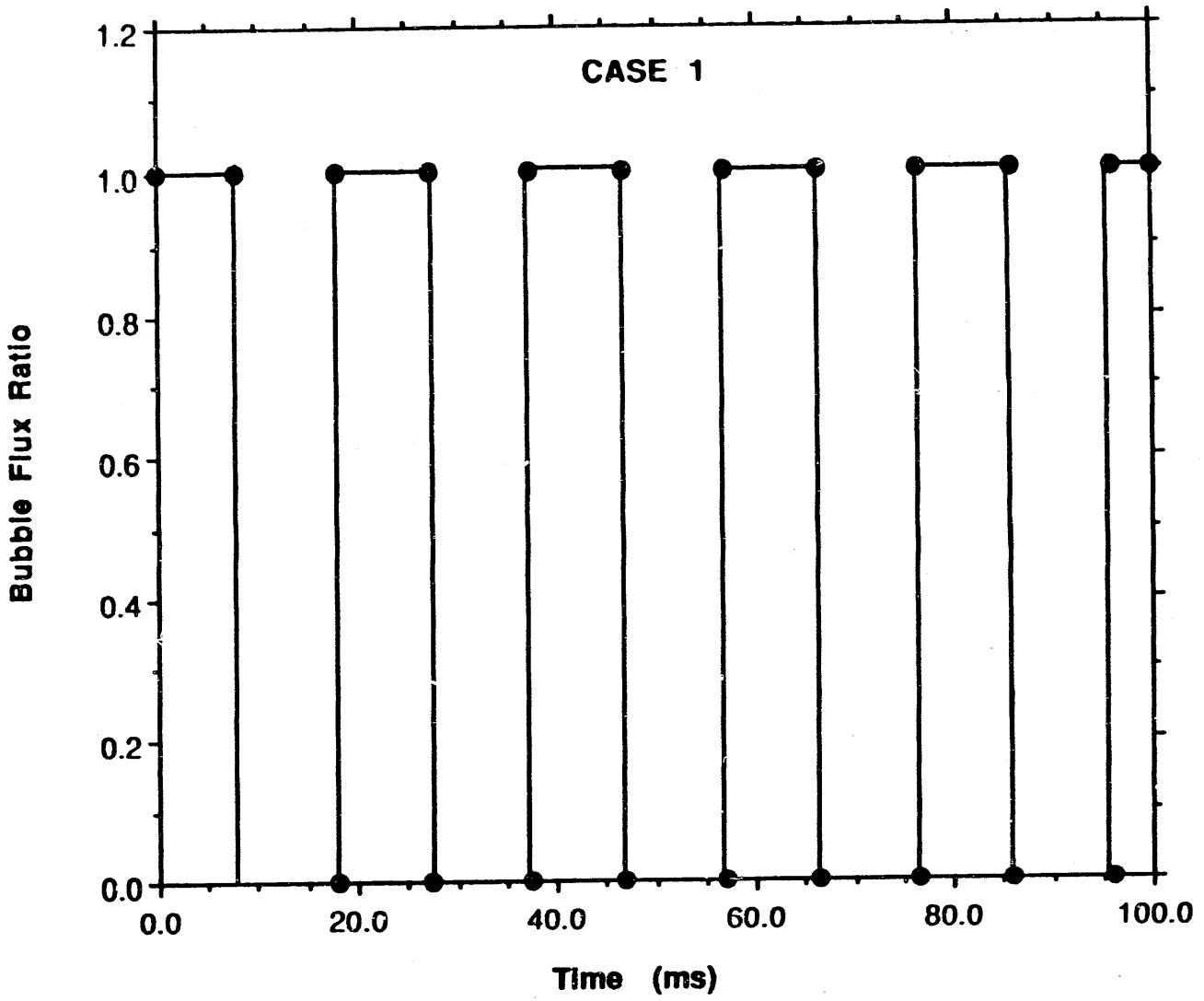

Fig. 5. Bubble flux ration for Case 1.

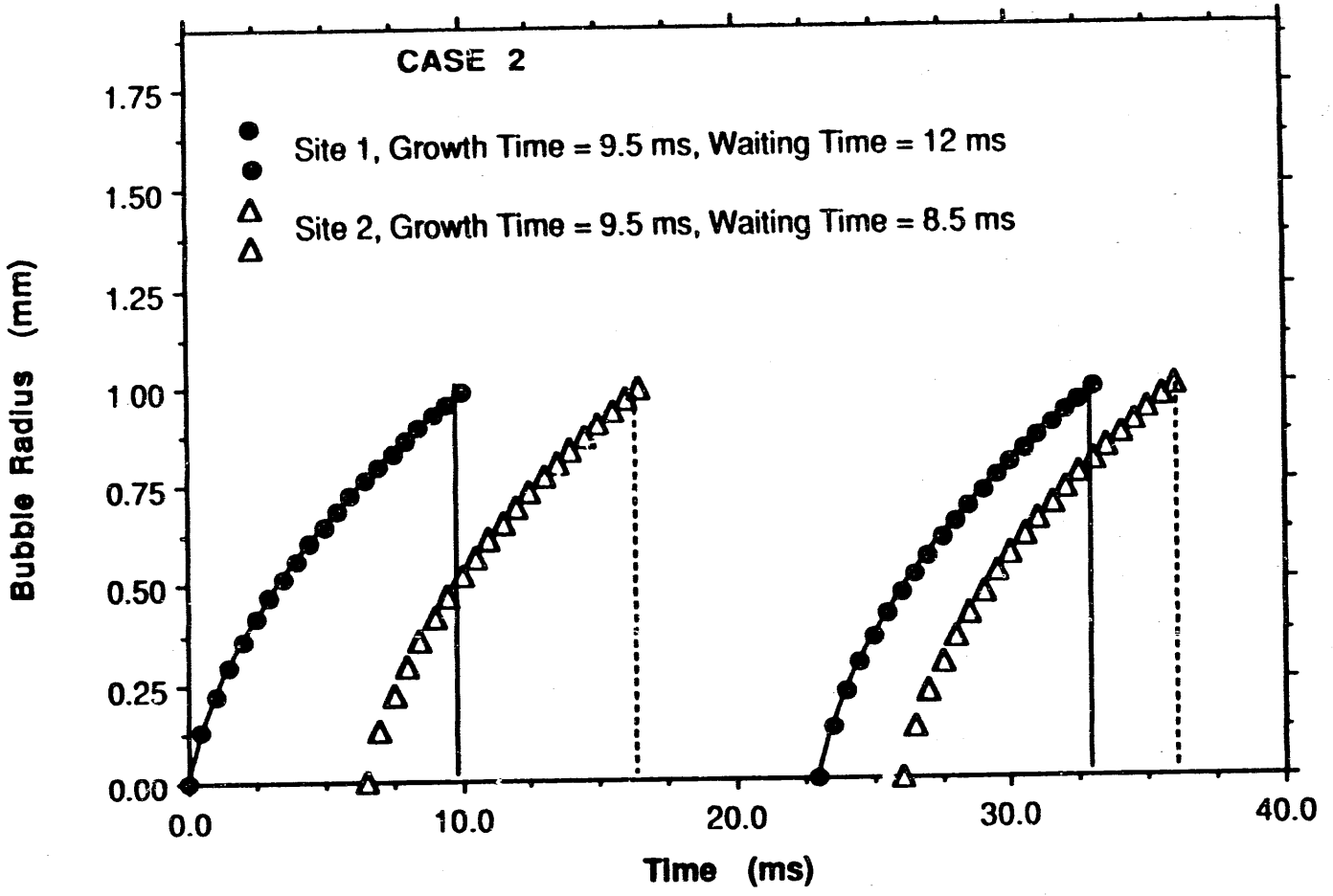

Fig. 6. Bubble behavior for Case 2.

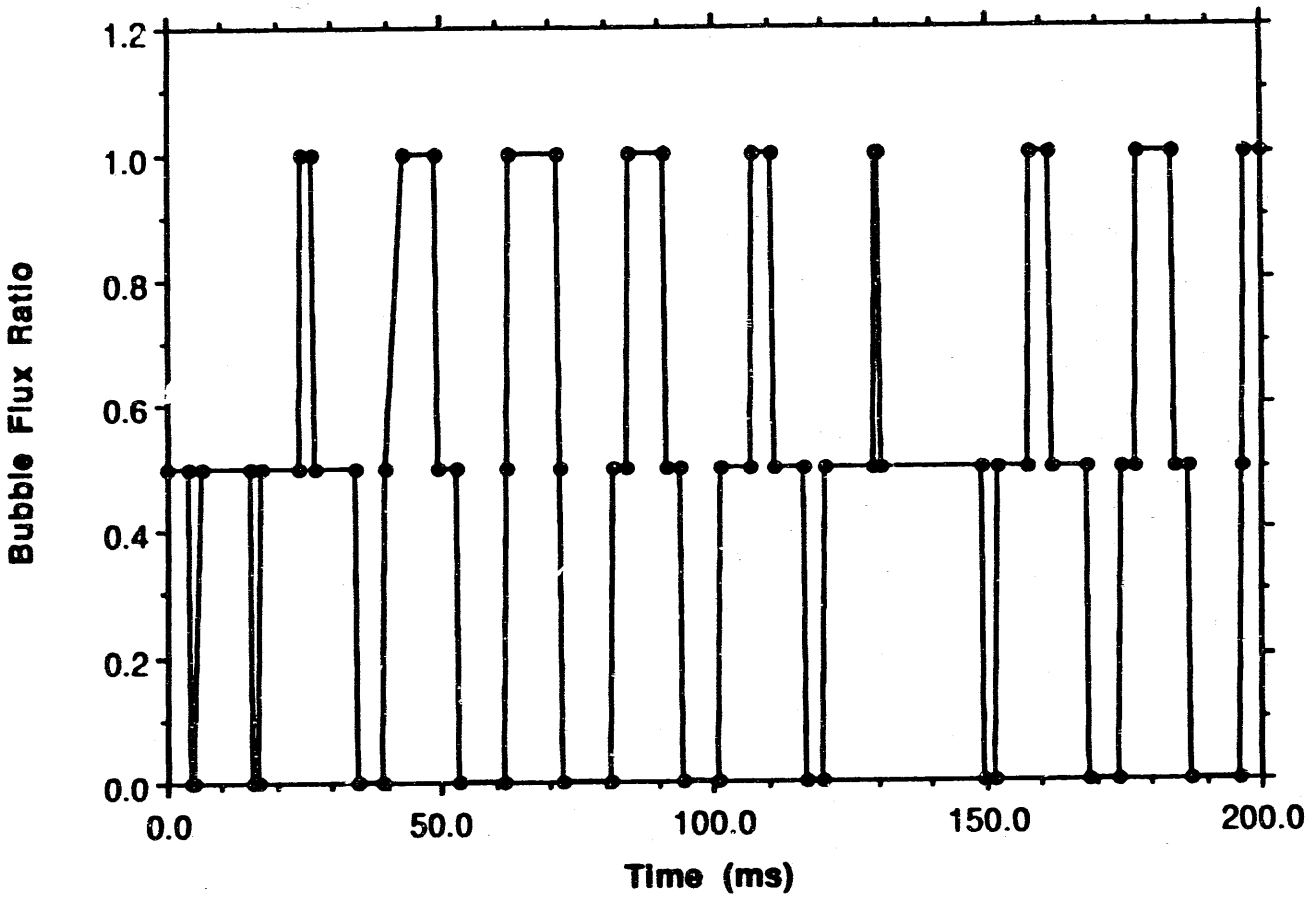

Fig. 7. Bubble behavior for Case 2.

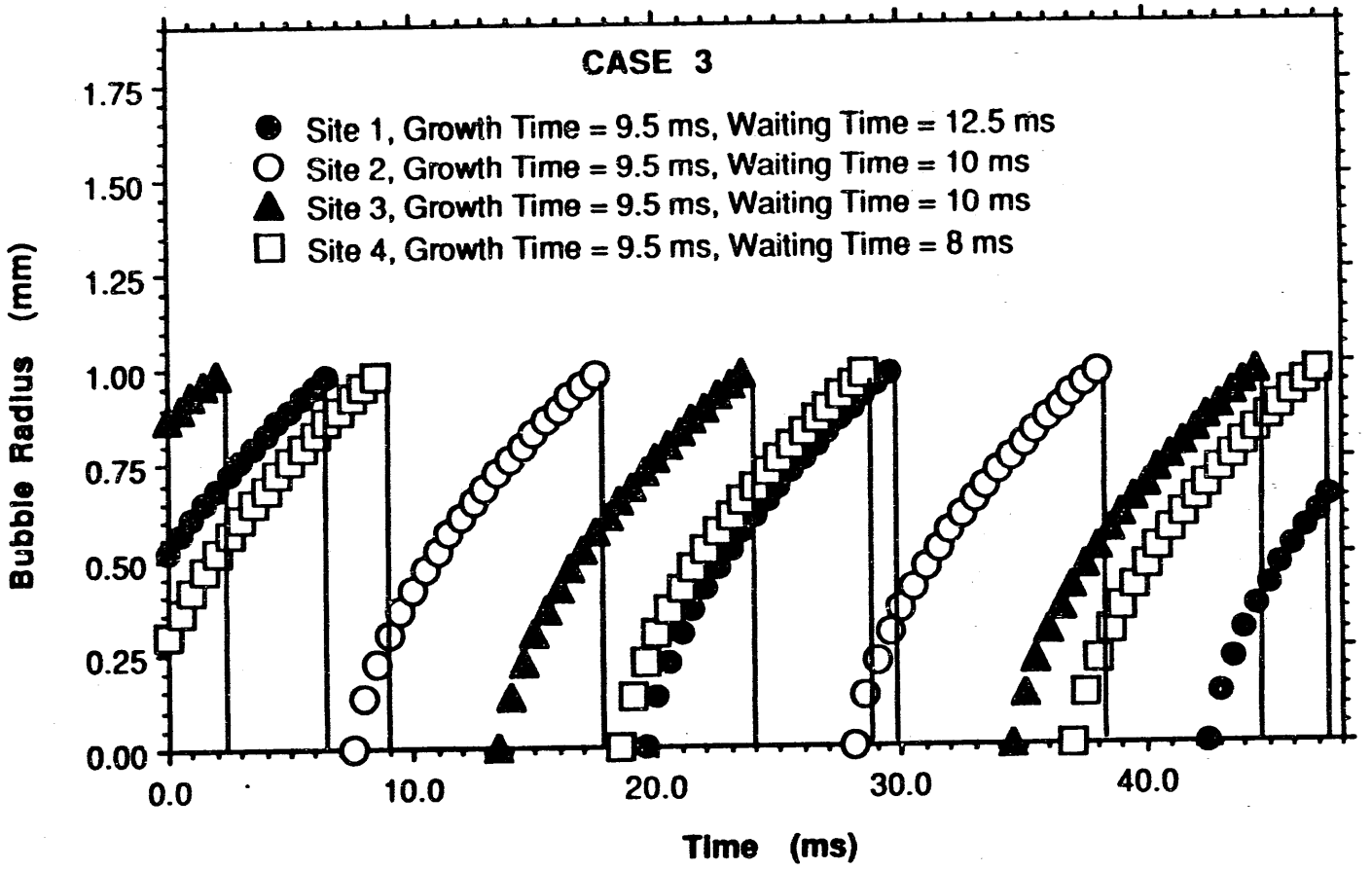

Fig. 8. Bubble behavior for Case 3.

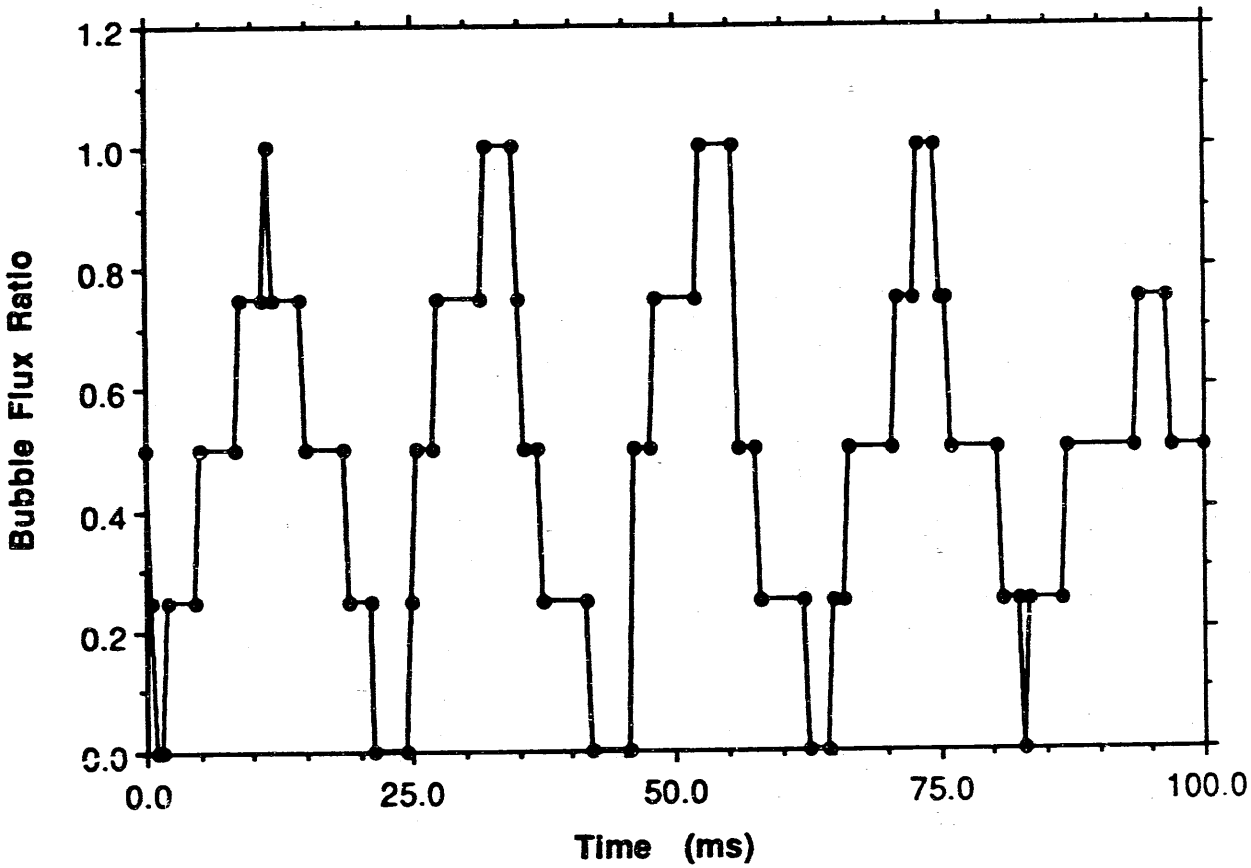

Fig. 9. bubble flux ration for Case 3

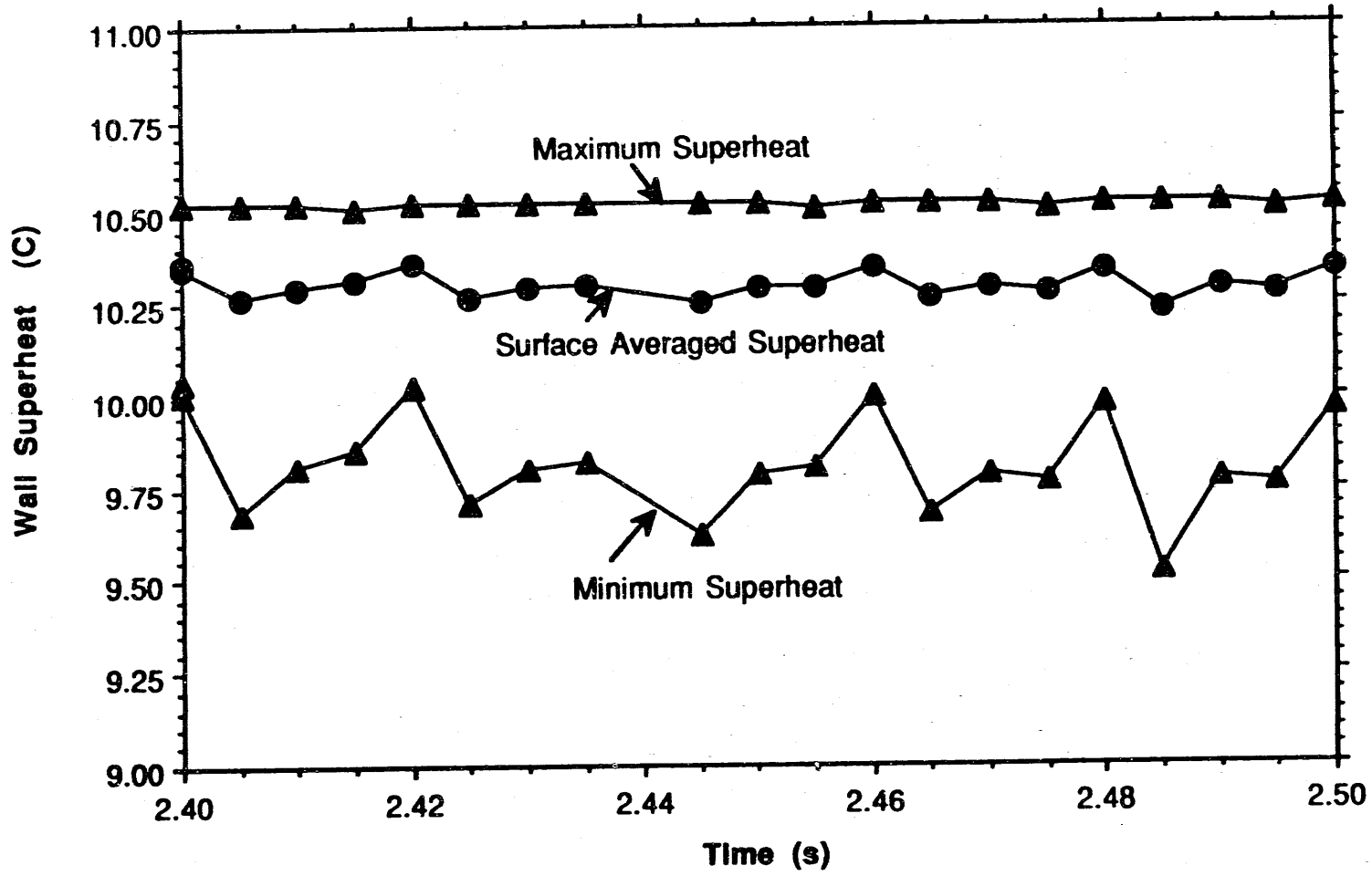

Fig. 10. Wall superheat behavior for Case 1.

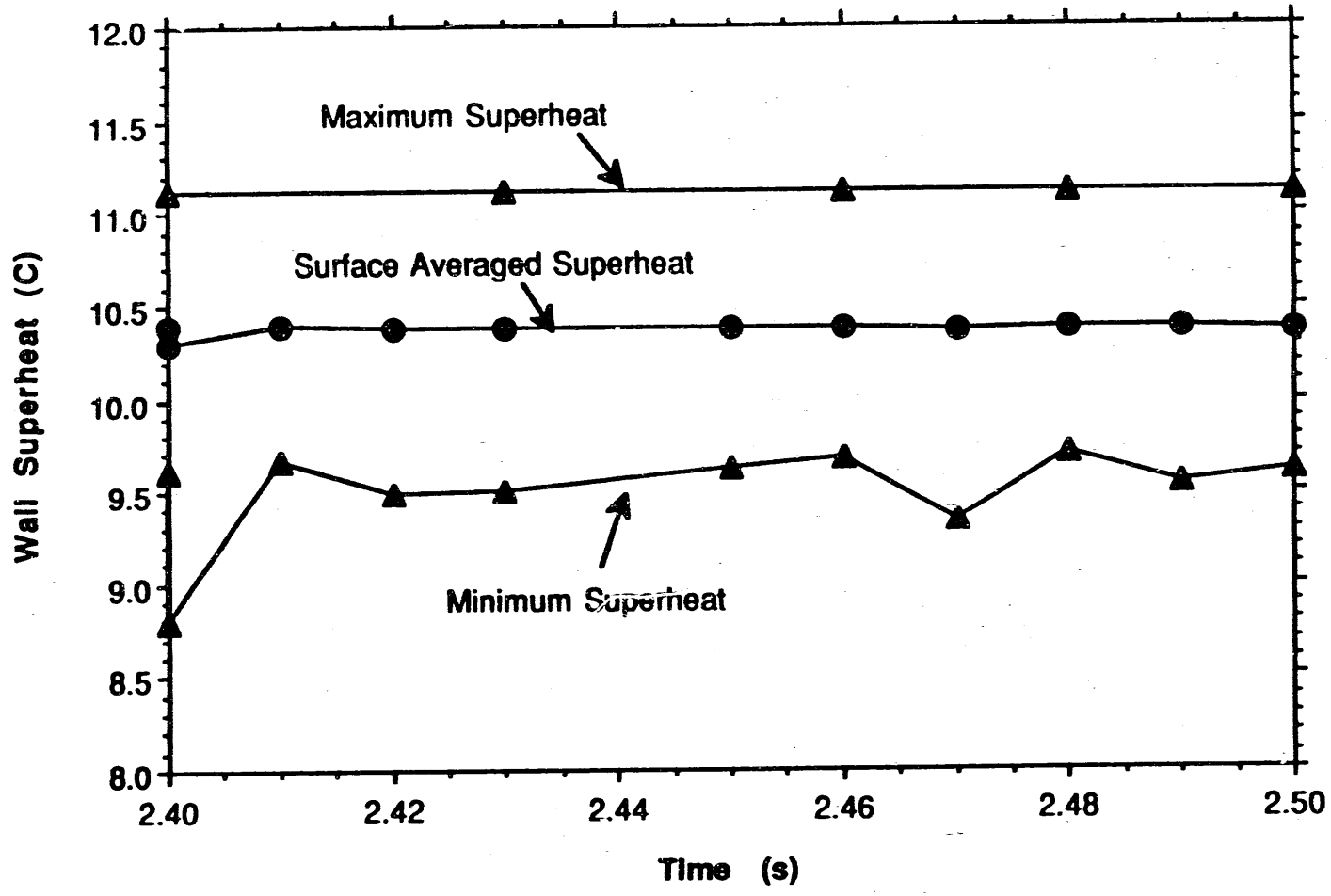

Fig. 11. Wall superheat behavior for Case 2.

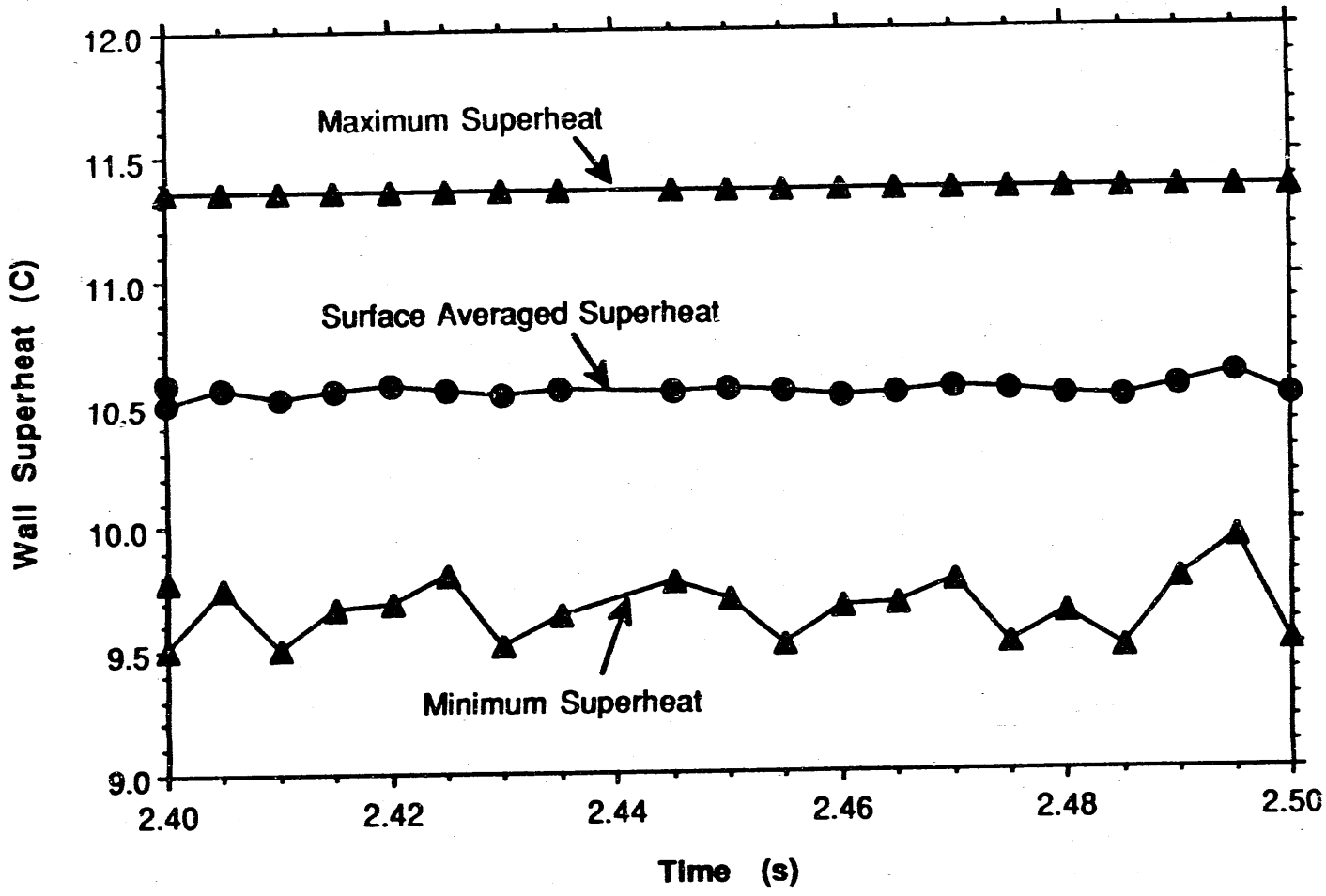

Fig. 12. Wall superheat behavior for Case 3.

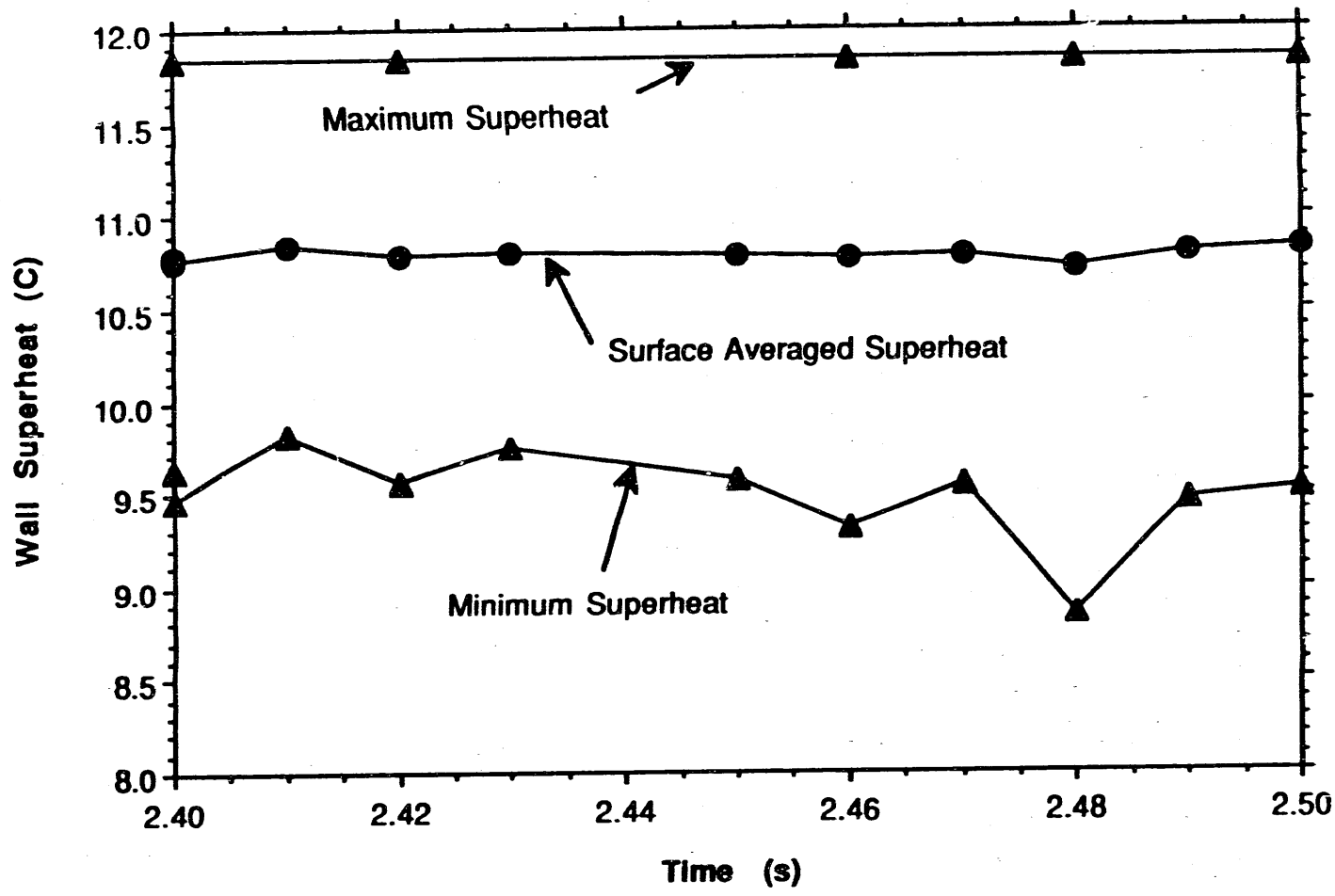

Fig. 13. Wall superheat behavior for Case 4.

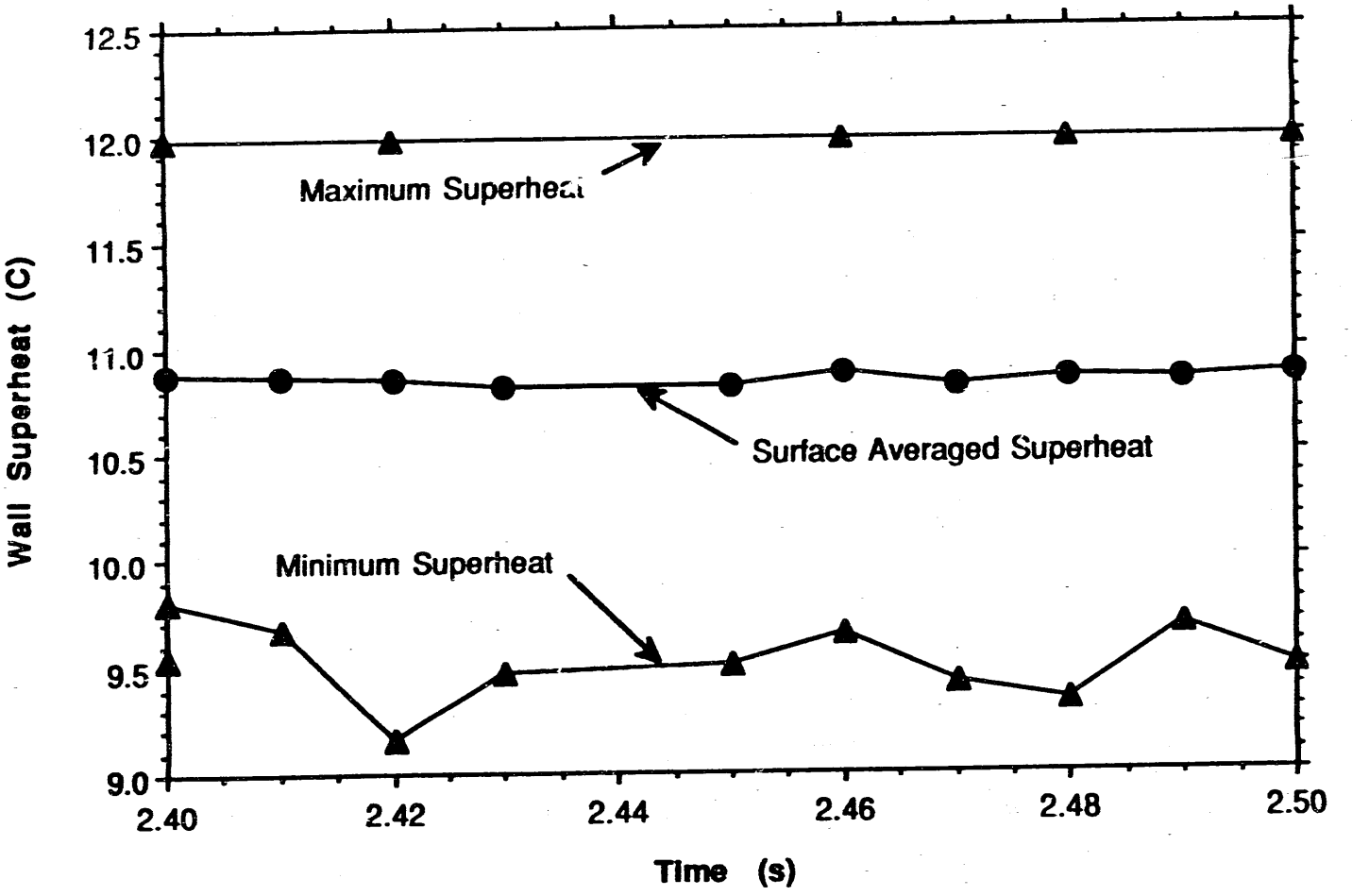

Fig. 14. Wall superheat behavior for Case 5.

END

DATE FILMED

06 / 10 / 91